^{23}Na Nuclear Magnetic Resonance and ^{1}H Pulsed Gradient Spin−Echo Detection of the Critical Concentration Corresponding to the Isotrope/Nematic Transition within Aqueous Dispersions of Charged Anisotropic Nanoparticles

P. Porion,* M. Al-Mukhtar, A. M. Faugère, and A. Delville

CRMD, CNRS, 1b rue de la Férollerie, 45071 Orléans Cedex 02, France

Received: January 28, 2004; In Final Form: April 29, 2004

With the use of ^{23}Na nuclear magnetic resonance spectroscopy and ^{1}H pulsed field gradient attenuation, we have determined the critical concentration at which the isotrope/nematic transition occurs within aqueous dispersions of synthetic Laponite clay used as a model of a charged anisotropic colloid. The dense macroscopic clay samples were prepared by oedometric compression, leading to a critical concentration for the isotrope/nematic transition significantly higher than that determined previously by using birefringence detection within capillary tubes. The increase of the nematic ordering detected by NMR as a function of the clay concentration is more progressive than the sharp ordering predicted by numerical simulations of the isotrope/nematic transition of rigid disks. This difference may result from some size and shape heterogeneities of the Laponite clay samples or from the competition between the relative orientation of the particles induced by the excluded volume and the electrostatic interactions.

I. Introduction

The isotrope/nematic transition has been previously reported for a large variety of dispersions of organic,[1−3] biological,[4−6] and mineral[7−10] anisotropic particles of any shape (rods and/or disks). As predicted by Onsager,[11] this first-order phase transition is driven by entropic effects: the anisotropic solid particles organize themselves, reducing their rotational entropy in order to optimize their translational entropy. The same self-organization was reported for a large variety of charged colloids, including metallic oxides and clay minerals, but a controversy still persists in the case of aqueous dispersions of synthetic Laponite clay. While some authors claim to have detected nematic organization of dilute Laponite dispersions[12−16] (less than 4% w/w) within capillary tubes, the direct observation of larger samples fails to exhibit, at the same clay concentration, a macroscopic phase separation[17] or a parallel alignment[18] of the particles. Furthermore, investigations using ^{23}Na nuclear magnetic resonance spectroscopy[19] and ^{1}H pulsed field gradient echo attenuation[20,21] also failed to exhibit nematic ordering within such bulk and dilute (less than 4% w/w) Laponite samples.

We have thus prepared, by gradual compression, a set of bulk equilibrium samples of Laponite aqueous dispersions in order to check for the possible occurrence of an isotropic/nematic transition. Numerical simulations of the electrostatic coupling between two isolated charged disks mimicking Laponite particles have indeed revealed a preferential organization of the clay particles perpendicular[22,23] to each other. As a consequence, the optimization of the electrostatic contribution to the free energy of these charged particles may cancel the entropic contribution resulting from their excluded volume interactions. By contrast with other clays or metallic oxides,[7−10] Laponite particles, with their small aspect ratio[24] (diameter/thickness ∼30) and their strong electrostatic coupling (∼1000 electric charges per particle)[17] are ideal probes to illustrate how the soft core electrostatic repulsion alters the thermodynamical behavior expected on the basis of theoretical treatments including only the excluded volume hard core repulsion.

In this study, the critical clay concentration corresponding to the occurrence of nematic ordering is determined by using ^{23}Na and ^{1}H nuclear magnetic resonance, in addition to the order parameter of nematic dispersions. Previous studies have already revealed the great sensitivity of ^{23}Na NMR to the macroscopic ordering[25] of Laponite dispersions. Because of their electrostatic coupling with the negatively charged clay surfaces, sodium counterions are strongly condensed in the electrostatic well in the direct vicinity of the Laponite particle:[22,23] 50% of the neutralizing sodium counterions are localized inside a cylinder of 30 Å thickness centered on the Laponite disk. Furthermore, because of the large asymmetry of their hydration sphere, these condensed sodium counterions feel a residual quadrupolar coupling[19] with the principal axis oriented perpendicular to the clay surface. As a consequence, the nematic ordering of the Laponite dispersion may be detected by the quadrupolar splitting of the resonance line of its sodium counterions. The nematic ordering of the clay dispersions was also detected by measuring the water mobility by using ^{1}H pulsed field gradient echo attenuation.[20,21] Because of the aspect ratio of the Laponite particle (300 Å diameter, 10 Å thickness),[24] the tensor describing the water self-diffusion within nematic dispersions becomes anisotropic with a transverse mobility (i.e., along the clay director) smaller than the longitudinal mobility (i.e., parallel to the clay surface). Both procedures are used to detect the critical clay concentration at which nematic ordering occurs and also to quantify the degree of the clay organization.

II. Material and Methods

A. Sample Preparation. Laponite RD was purchased from Laporte and used without purification. Laponite clay was dispersed in an electrolyte solution (NaCl 10^{-2} M, NaOH 10^{-4}

* To whom correspondence should be addressed. E-mail: porion@cnrs-orleans.fr.

10.1021/jp049617j CCC: $27.50
Published on Web 06/22/2004

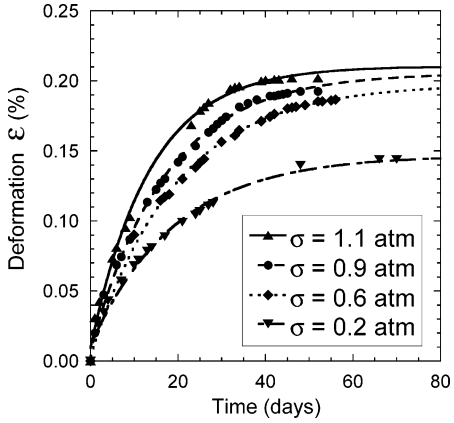

Figure 1. Gradual deformation ϵ of the Laponite dispersions under oedometric uniaxial compression σ.

M) to prevent dissolution of the clay particles.[26] Dilute samples (up to 5% w/w) were directly prepared by dispersion in water. Concentrated samples were obtained by oedometric compression leading to density (up to 92% w/w). The final clay concentration of these samples was determined by their water loss at 80 °C under vacuum. The oedometer consists of a stainless steel cylinder (25 cm height, 3 cm inner diameter) closed by two membranes (0.1 μm from Osmonics) located on the bottom of the cylinder and in the head of the piston in order to facilitate water release during the compression of the suspension. Equilibration of the samples was typically achieved after 2 months (see Figure 1). The compression of the dense samples (more than 40% w/w) was performed by a gradual increase of the mechanical stress (σ).

B. NMR Measurements. ^{23}Na spectra were recorded on a DSX 360 Bruker spectrometer, with a static field of 8.465 T. A broad spectral width (1 MHz) and a fast acquisition procedure (time step 1 μs) were used because of the fast relaxation of these quadrupolar nuclei (spin = $^3/_2$). Typical pulse durations necessary to tilt the magnetization in the transverse detection plane were equal to 14 μs. The residual quadrupolar splitting of the ^{23}Na resonance spectra were initially deduced from a line shape analysis, by using numerical simulation to reproduce the time evolution of the different coherences during each elementary step of the RF pulse [$\pi/2$ pulse$-\tau$ delay$-$acquisition], where τ (i.e., 4.5 μs) is the irreducible time delay of our spectrometer. This procedure is necessary to reproduce the depletion of the resonance line close to the central line of the triplet (see Figure 2) because of the coherence relaxation which mixes the one-quantum coherences of all ranks.[25,27,28] The residual quadrupolar coupling (ω_Q) was also obtained by fitting (see Figure 3), during a classical spin$-$echo attenuation [$\pi/2$ pulse$-\tau/2$ delay$-\pi$ pulse$-\tau/2$ delay$-$acquisition], the variation of the echo amplitude as a function of the evolution time (τ)

$$M_x(\tau) = A\cos(\omega_Q\tau + \varphi)\exp(-\tau/T_2^{\text{fast}}) + B\exp(-\tau/T_2^{\text{slow}}) \quad (1)$$

where T_2^{fast} and T_2^{slow} are, respectively, the fast and slow transverse relaxation times of $^3/_2$ nuclei under slow modulation of their quadrupolar coupling. The value of the A/B ratio was found to be nearly equal to 60:40, as predicted by theory.[29] This procedure is more powerful than a direct fitting of the free induction decay signal recorded during a simple RF pulse, since it reduces the contribution from the heterogeneities of the static magnetic field.

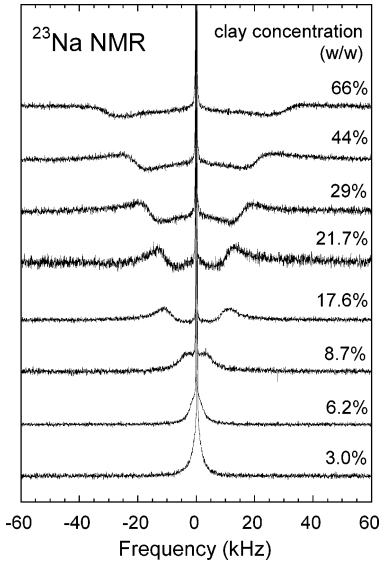

Figure 2. Influence of the clay concentration on the line shape detected by ^{23}Na NMR spectroscopy. All these spectra were obtained for the angle θ between the compression axis and the static magnetic field $\vec{B}_0$ equal to 0°.

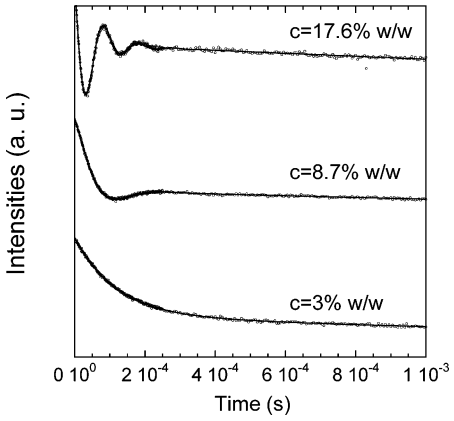

Figure 3. Influence of the clay concentration on the time variation of the transverse magnetization $M_x(\tau)$ of ^{23}Na nuclei during a spin$-$echo attenuation measurement.

^{1}H pulsed field spin$-$echo attenuation was used to measure the mobility of the water molecules within dense Laponite dispersions. The three principal directors of the water self-diffusion tensor are identified by determining the water mobility along six noncollinear directions.[20,21] The diffusion-weighted stimulated echo pulse sequence has been used (see Figure 4) with an echo attenuation according to[30,31]

$$\frac{I(q)}{I(0)} = \exp[-4\pi^2 q^2 \vec{e}_g^{\,T}\overleftrightarrow{D}\vec{e}_g(\Delta - \delta/3)] \quad (2)$$

where $q = \gamma g\delta/(2\pi)$, g is the intensity of the applied field gradient (varying between 0 and 1.2 T/m), $\vec{e}_g$ is its direction, δ is its duration, Δ is the diffusion time, γ is the gyromagnetic ratio of the nuclei, $\overleftrightarrow{D}$ is the self-diffusion tensor, and $I(q)$ and $I(0)$ are the echo intensities measured with and without the field gradient, respectively. Since the same pulse sequence, using the same coherence pathway, is used for recording the echo intensities with ($I(q)$) and without ($I(0)$) field gradient, they are both affected by the relaxation mechanisms of the water molecule, leading to the same echo attenuation [$I(0) \sim \exp(-2\tau_1/T_2)\ \exp(-\tau_2/T_1)$]. As a consequence, the water relaxation mechanisms do not contribute to the measured ratio

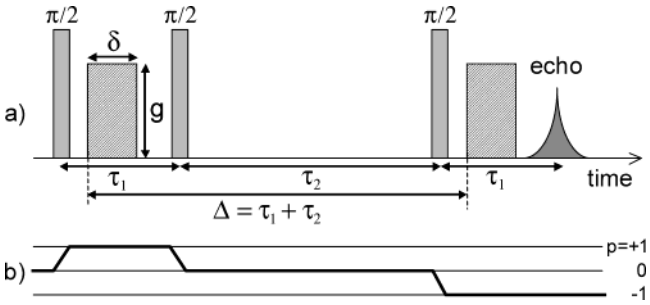

Figure 4. (a) Schematic view of the stimulated echo pulse sequence used for the measurement of the water self-diffusion. The three $\pi/2$ pulses produce a stimulated spin−echo at $2\tau_1 + \tau_2$. Between the second and third pulse, the magnetization is locked along the static magnetic field $\vec{B}_0$ during the time τ_2. The diffusion time is $\Delta = \tau_1 + \tau_2$. (b) Coherence transfer pathway ($p = 0 \rightarrow +1 \rightarrow 0 \rightarrow -1$) resulting from an adequate phase cycling.

$I(q)/I(0)$. The maximum value of the magnetic field gradient (1.2 T/m) corresponds to wavenumbers q smaller than 5×10^4 m^{-1}. The diffusion measurements are thus macroscopic and result from averages over a sample size larger than 20 μm. The samples are macroscopic cylinders (thickness 4 mm, diameter 4 mm) cut into the dense aqueous dispersions of clay. The diffusion experiments were performed on a Bruker DSX 100 spectrometer equipped with a microimaging probe (Micro5 Bruker) with gradient coils in three perpendicular directions used to generate magnetic field gradients along any arbitrary direction $\vec{e}_g$. The temperature was fixed at 296 K.

III. Results and Discussion

^{23}Na is a quadrupolar nucleus with spin $^3/_2$; the relaxation of its transverse magnetization is monitored by the loss of memory of the average quadrupolar coupling felt by the sodium counterion. When the time scale characterizing this decorrelation is larger than the inverse of the resonance angular velocity (the so-called slow modulation regime),[29] two relaxation times and two superimposed resonance lines are detected for a single spin population (see Figures 3 and 2, respectively, for a clay concentration smaller than 8.7%). First, a thin resonance line, which corresponds to the slow relaxation mechanism, originates from the transition between the $-^1/_2 \leftrightarrow ^1/_2$ spin levels and represents 40% of the total magnetization. Second, a broad resonance line, which corresponds to the fast relaxation mechanism, originates from the transitions between the $-^3/_2 \leftrightarrow -^1/_2$ and the $^1/_2 \leftrightarrow ^3/_2$ spin levels and represents 60% of the total magnetization. Such behavior is detected within the dilute Laponite dispersions (up to 6.2% w/w) because the mechanism responsible for the slow modulation of the quadrupolar coupling is the diffusion of the sodium counterions within the dispersion. A molecular model of the clay/water interface has indeed shown that the sodium counterions located near the clay surface feel a strong residual electrostatic field gradient ($Vzz \sim (7 \pm 3) \times 10^{19}$ V/m^2), with the $\mathbf{e}_z$ axis oriented along the clay director.[19] This residual electric field gradient results from the anisotropy of the distribution of the electric charges at the clay/water interface and from the distortion of the hydration shell of the condensed cations.[19] As a consequence, the only possibility for initially condensed sodium counterions to lose the memory of their initial quadrupolar coupling is to desorb from the clay surface, diffuse into the dispersion, and hit another clay particle with an orientation fully decorrelated from the orientation of the initial clay particle.[19] As a consequence, the correlation time detected by ^{23}Na relaxometry within dilute Laponite dispersions (typically10^{-6} s)[32] is the fingerprint of the spatial extent

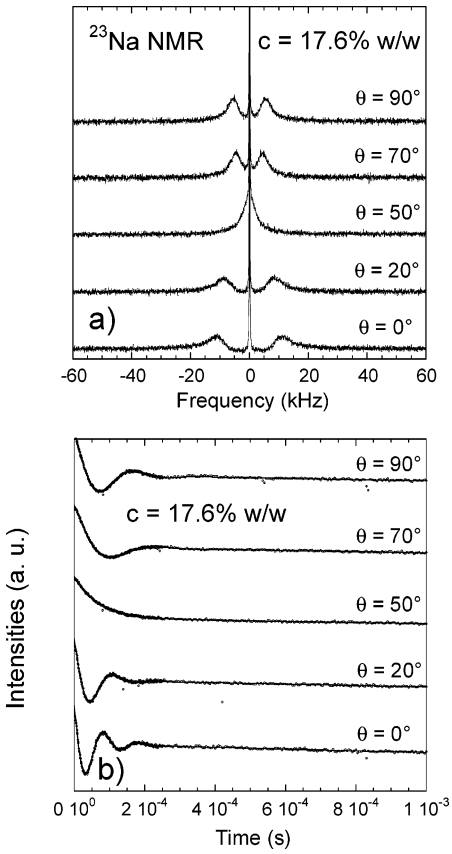

Figure 5. (a) Angular variation of the splitting of the ^{23}Na NMR line shape and (b) time evolution of the transverse magnetization $M_x(\tau)$ within a nematic Laponite dispersion ($c = 17.6\%$ w/w).

(typically 300 Å, i.e., the size of the Laponite particle) of locally ordered microdomains within dilute (up to 6.2% w/w) Laponite dispersions.

If the orientation of the clay particles is fully random, these thin and broad ^{23}Na resonance lines are superimposed and no residual quadrupolar coupling is detected for dilute (up to 6.2% w/w) and macroscopically isotropic dispersions,[19,32] but above that limiting clay concentration, a splitting of the broad component emerges[25] (see Figure 2) and gradually increases as a function of the clay density.[25] This residual splitting is the consequence of a nematic ordering of the clay dispersion. As shown in Figure 5a, the splitting measured at a given clay concentration varies continuously as a function of the orientation of the compression axis within the magnetic field. One also notes a nearly perfect cancellation of the residual splitting at the magic angle θ_M ($\theta_M \approx 54.7°$), with ^{23}Na resonance lines then equivalent to that detected for isotropic samples. Equivalent results are obtained from the angular variation of the time evolution of the transverse magnetization (see Figure 5b). Figure 6 resumes the detected angular variation of the residual quadrupolar coupling which leads, after normalization by the maximum quadrupolar splitting, to an order parameter varying according to the expected $0.5|(3\cos^2\theta - 1)|$ relationship. This perfect matching is the consequence of the macroscopic ordering of the Laponite orientation along a single nematic director. From the detection of the residual quadrupolar splitting, we localize at $7 \pm 1\%$ w/w the critical clay concentration at which the isotrope/nematic transition occurs in Laponite dispersions for an ionic strength equal to 10^{-2} M. This critical Laponite concentration is significantly larger than the value detected initially by birefringence within capillary tubes (5% w/w[13] or even 2% w/w[12]) and later confirmed by small angle X-ray

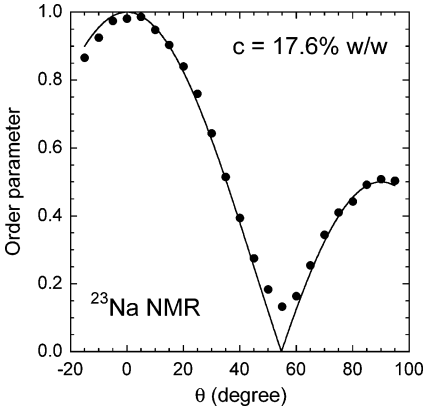

Figure 6. Variation of the order parameter $\omega_Q(\theta)/\omega_Q(0°)$ resulting from the analysis of the residual quadrupolar splitting as displayed in Figure 5. The curve represents the best fit of the function $(^1/_2)|3\cos^2(\theta) - 1|$.

scattering.[15,16] We believe that such discrepancies result from the macroscopic alignment of the Laponite particles due to the shear stress induced by the flow of the suspension into the capillary tubes used for these experiments. By contrast, the maximum residual coupling is detected by ^{23}Na NMR within the nematic dispersions when the direction of the magnetic field is oriented parallel to the direction of the compression applied to the clay samples. Since the director of the principal axis of the electrostatic field gradient felt by the condensed sodium counterions is oriented along the clay director, one concludes that these oedometric compressions align the directors of the anisotropic particles parallel to the compression axis. As a consequence, this ordering is not expected to be induced by the water flow through the clay sample.

The great sensitivity of the detection of the splitting of the ^{23}Na resonance line results from the order of magnitude of the average residual coupling characterizing the hydrated sodium counterions in the vicinity of the Laponite surface

$$\omega_Q^{obs} = p_F\omega_Q^F + p_B\omega_Q^B \tag{3a}$$

with

$$\omega_Q^F \equiv 0 \tag{3b}$$

$$\omega_Q^B = |\langle P_2(\cos(\theta)\rangle|\omega_Q^{Max} \tag{3c}$$

and

$$\omega_Q^{Max} = (2\pi eQV_{zz}/h) = (1.2 \pm 0.6) \times 10^6\ s^{-1} \tag{3d}$$

where p_F and p_B are respectively the fractions of free and condensed sodium counterions, θ is the angle between the static magnetic field and the clay director, and $|\langle P_2(\cos(\theta)\rangle| = |\langle 0.5(3\cos^2\theta - 1)\rangle|$ is the average order parameter of the platelet suspension.

Since 50% of the sodium counterions are condensed in the vicinity of the Laponite particles and can feel this maximum splitting, a residual splitting ($\omega_Q^{obs} \sim 10^4\ s^{-1}$) remains detectable even if the average ordering of the clay particles is weak ($|\langle P_2(\cos(\theta)\rangle| \sim 10^{-2}$). This minimum detection level is limited by the order of magnitude of the fast component of the transverse relaxation rate measured for ^{23}Na in the presence of Laponite ($R_2^{fast} = 1/T_2^{fast} \sim 10^4\ s^{-1}$).[19] No splitting of these two broad resonance lines (see Figure 2) may indeed be detected if it is lower than the intrinsic broadening of the lines. Under such conditions, a large increase of the sensitivity will result from

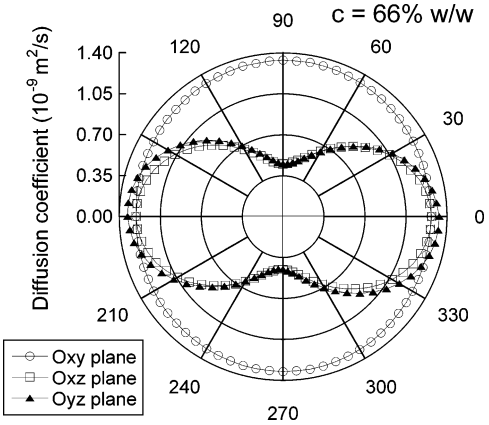

Figure 7. Water mobilities detected by ^{1}H PFGE attenuation within the nematic Laponite dispersion (c = 66% w/w). The water mobility is measured within each of the three planes defined by two of the principal axes characterizing the tensor describing the water self-diffusion (see text).

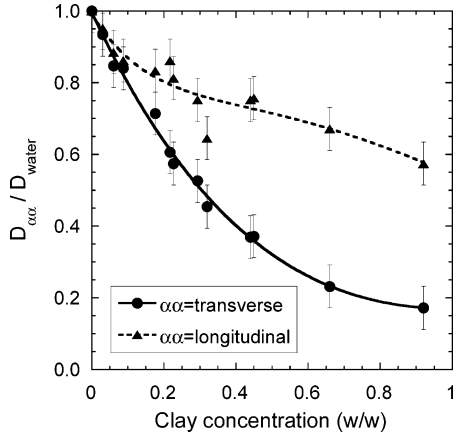

Figure 8. Variation of the longitudinal and transverse water self-diffusion coefficient as a function of the clay concentration.

the detection by using double-quantum filtering in order to select only these two broad components with an opposite phase.[33−36]

The detection of this isotrope/nematic organization of the Laponite dispersions is also confirmed by the detection of the anisotropy of the tensor describing the self-diffusion of the water molecules.[20,21] Since the time scale investigated by the ^{1}H pulsed field gradient echo attenuation procedure is equal to 20 ms, the apparent water mobility results from an average over macroscopic domains of the order of magnitude of 10 μm and the water mobility probes the macroscopic tortuosity of the porous network limited by the solid clay particles. To further illustrate the anisotropy of the solvent mobility within dense phases, the self-diffusion coefficient is also measured by gradually varying the direction of the field gradient $\vec{e}_g$ within the three planes defined by two of the previously identified principal directions (noted $\vec{e}_\alpha$ and $\vec{e}_\beta$) of the diffusion tensor (Figure 7). The measured diffusion coefficient varies according to

$$D_{meas}(\phi) = \vec{e}_g^T D \vec{e}_g = D_{\alpha\alpha}\cos^2(\phi) + D_{\beta\beta}\sin^2(\phi) \tag{4}$$

where ϕ is the angle between $\vec{e}_\alpha$ and $\vec{e}_g$ and $D_{\alpha\alpha}$ and $D_{\beta\beta}$ are the eigenvalues of the tensor **D** corresponding, respectively, to the principal directions $\vec{e}_\alpha$ and $\vec{e}_\beta$.

For dilute clay dispersions (up to 8.7% w/w), the water mobility does not reveal preferential directions (see Figure 8) and the distribution of the Laponite particles within the sampling volume appears isotropic. Above that limiting clay concentra-

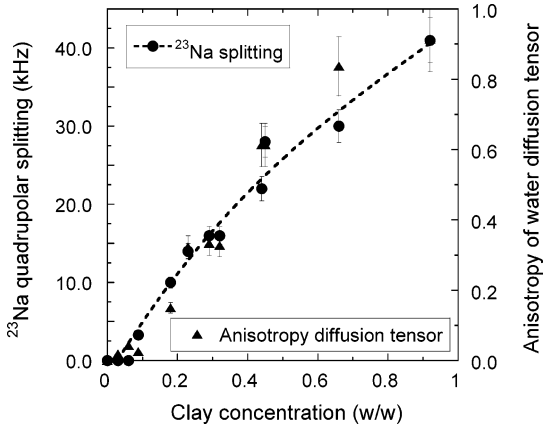

Figure 9. Detection of the isotrope/nematic phase transition within aqueous Laponite dispersions by measuring the ^{23}Na residual splitting and the anisotropy of the water mobility as a function of clay concentration *c*.

tion, the ratio of the longitudinal and transverse cross sections of the Laponite particles is large enough to exhibit a clear anisotropy of the water self-diffusion (see Figure 8), confirming the existence of a macroscopic nematic phase. A simple measurement of the water self-diffusion anisotropy (see Figure 9) is given by the anisotropy ratio of the self-diffusion tensor

$$\frac{D_{\text{long}} - D_{\text{trans}}}{(1/3)\sum_{\alpha} D_{\alpha\alpha}} = \frac{D_{\text{long}} - D_{\text{trans}}}{(1/3)(2D_{\text{long}} + D_{\text{trans}})} \qquad (5)$$

since the transverse mobility (i.e., perpendicular to the clay surface) corresponds to a single eigenvalue of the self-diffusion tensor, while two equivalent mobilities characterize the longitudinal diffusion (parallel to the clay surface).

Surprisingly enough, both procedures (^{23}Na residual splitting and water self-diffusion anisotropy) lead to nearly equivalent conclusions (see Figure 9). On one hand, the residual splitting of the ^{23}Na resonance line results from the average quadrupolar coupling felt by these sodium counterions condensed in the vicinity of the clay particles (see eq 3a−d). As a consequence, the progressive variation displayed by the residual ^{23}Na splitting as a function of the clay concentration (see Figure 9) may result from two simultaneous phenomena: the increase of the degree of ordering of the clay dispersion and the increase of the fraction of condensed sodium counterions. On the other hand, the anisotropy of the water self-diffusion is a direct measurement of the ordering of the clay suspension, independent of the fraction of condensed counterions or the orientation of the clay sample, within the static magnetic field. Both experiments lead to equivalent results (see Figure 9) if and only if the fraction of condensed sodium counterions is constant during the compression of the Laponite dispersion. For polyelectrolytes (i.e., linear charged colloids), the fraction of condensed counterions predicted by the condensation theory[37,38] is independent of the salt and colloid concentration. Monte Carlo simulations[39,40] have recently confirmed the validity of that prediction in the case of lamellar charged colloids by calculating the distribution of the sodium counterions in the electrostatic wells located in the vicinity of the clay particles. Increasing the aspect ratio of the clay particles should enhance the anisotropy of the water mobility, leading to unidirectional diffusion barriers with a high retention power. The same detection of the residual quadrupolar coupling of condensed counterions may be performed for other quadrupolar nuclei (^{7}Li, ^{85}Rb, ^{87}Rb, etc.).

Both experimental procedures (^{23}Na residual splitting and water self-diffusion anisotropy) indicate a very gradual increase of the nematic ordering of the clay dispersion. Numerical simulations of rigid disks were already performed[41] to test the isotrope/nematic first-order transition of anisotropic colloids. The variation of the ordering of the Laponite dispersions as a function of the clay concentration (Figure 9) exhibits two significant differences with the data resulting from numerical simulations of rigid disks (see Figure 5 in reference 41):

(i) First, the nematic ordering was shown to occur[41] at a reduced disk concentration $\rho^* = N(d/L)^3 \sim 3.9$ (where d is the platelet diameter and L is the length of the simulation cell), corresponding to a critical clay concentration (0.28 w/w) much higher than the value detected by NMR.

(ii) Second, the variation of the nematic ordering was sharper for rigid disks. As an example, the average order parameter ($\langle P_2(\cos(\Theta))\rangle$) varies from 0.02 to 0.86 when the reduced disk concentration ρ^* increases[41] from 3.2 to 8.2, i.e., when the corresponding clay concentration increases from 0.23 to 0.58 w/w. As shown in Figure 9, the order parameter detected by NMR within Laponite dispersions increases only roughly from 0.05 to 0.5 in the same range of clay concentration (between 0.1 and 0.45 w/w), while 90% ordering requires a clay concentration near 1 w/w.

Many factors may explain these differences without invalidating the occurrence of the Onsager first-order isotrope/nematic phase transition. First, including the contribution of the ionic diffuse layer into the apparent thickness of the clay particles[42] was shown to shift to lower value the critical concentration corresponding to the isotrope/nematic transition. The strong condensation of the neutralizing counterions on the basal surface[22] of the clay particles may be used to justify such a crude approximation. However, the optimization of the electrostatic contribution to the free energy of two charged disks[23] and cylinders[43−47] was recently shown to lead to a relative perpendicular orientation of their directors by contrast with their parallel alignment induced by excluded volume interactions. As a consequence, the electrostatic contribution to the free energy of a large collection of charged disks[48] may alter the sharp isotrope/nematic transition expected for rigid bodies. We perform now numerical simulations in order to quantify how the optimization of the electrostatic coupling within a large collection of charged disks modifies their relative orientation. Another factor restricting the sharpness of such a isotrope/nematic transition is the polydispersity of the particle sizes[49] and shapes.[50,51] Laponite RD is a synthetic clay with a limited size heterogeneity (diameter 250 ± 50 Å).[24] In that context, numerical simulations of a large collection of rigid bodies should be very useful for determining the influence of particle sized heterogeneity on their mutual ordering. Furthermore, the ionic strength is an important parameter modulating the range of the electrostatic coupling between charged colloids[40,52] and thus the possible competition between electrostatic and excluded volume effects. During our oedometric compressions, no reservoir is used to stabilize the ionic strength. Under such conditions, and because of the Donnan exclusion phenomenon,[40,52] the salt concentration is expected to decrease in the suspension during its compression with a simultaneous increase of the salt concentration of the eluated liquid phase. We thus expect an increase of the screening of the electrostatic repulsion between the charged colloids during the compression. In order to quantify this phenomenon, let us assume a chemical equilibrium between the salt molecules at both sides of the membrane, i.e., between the compressed suspension (noted 1) and its eluate (noted 2).

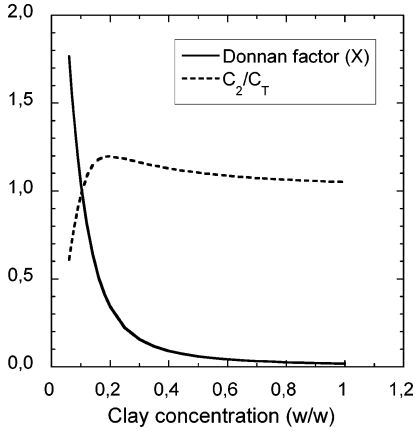

Figure 10. Variation of the Donnan exclusion factor (X) and the salt ratio of the eluate (C_2/C_T) estimated as a function of the sample compression (see text).

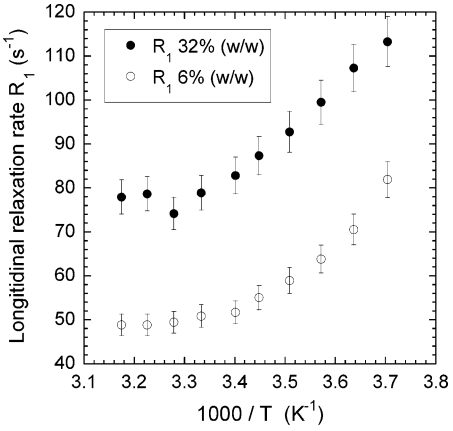

Figure 11. Temperature variation of the ^{23}Na longitudinal relaxation rate (R_1) within dense isotrope ($c = 6\%$ w/w) and nematic ($c = 32\%$ w/w) Laponite dispersions.

From the conservation of the total volume and the salt quantity, we obtain

$$V_1 + V_2 = V_T \tag{6a}$$

$$c_1V_1 + c_2V_2 = c_TV_T \tag{6b}$$

where c_T is the initial salt concentration (10^{-2} M), V_T is the initial volume, and c_i is the salt concentration of phase i with a volume V_i. From the Donnan exclusion phenomenon[40,52] we obtain

$$\frac{c_1}{c_2} = X \leq 1 \tag{6c}$$

Equations 6a−c summarize to

$$\frac{c_2}{c_T} = \frac{1}{X + \frac{V_2}{V_T}(1 - X)} \tag{7}$$

In order to evaluate the Donnan fraction X, let us replace the dispersion of charged disks by a collection of infinite parallel charged lamellae at the same solid concentration and surface charge density. Under the approximation of a strong electrostatic coupling, we obtain[52]

$$\frac{c_1}{c_2} = \frac{(\kappa D)^2}{8\pi^2}\left(1 + \frac{3}{F}\right) \tag{8}$$

where D is the interlamellar separation, $F = \pi L_B \Sigma D$, Σ is the surface charge density (7×10^{-3} Å^{-2} for Laponite clay), L_B is the Bjerrum length ($L_B = e^2/(4\pi\epsilon_0\epsilon_r kT)$), and κ^{-1} is the Debye screening length ($\kappa = \sqrt{8\pi L_B c_2}$). Note that the Debye screening length is determined from the salt concentration in the reservoir,[52] i.e., within the eluate which remains in contact with the membrane. Figure 10 is obtained by solving eqs 7 and 8 in a self-consistent manner. At an ionic strength around 10^{-2} M, the validity of eq 8 is restricted to interlamellar separations smaller than 150 Å, i.e., to Laponite concentrations larger than 0.18 w/w. At larger separations, instead of diverging (see Figure 10) the exact Donnan factor tends toward unity[52] and no salt separation occurs. As shown in Figure 10, the salt increase of the eluate is always smaller than 20%, corresponding to a maximum increase of 10% of the screening of the electrostatic coupling between the charged colloids. As a consequence, with an initial salt concentration of 10^{-2} M, the salt density of the eluate may be considered as constant with a good degree of accuracy. This conclusion is far from being valid for clay dispersions prepared by solvent evaporation.[12,15]

Neither the direct visual inspection of the Laponite dispersions,[17,18] nor the ^{23}Na NMR relaxation measurements, nor the ^{1}H pulsed field gradient measurements of the water mobility exhibit evidence of a phase coexistence as expected for the first-order isotrope/nematic phase transition predicted by Onsager.[11,41,42] Such existence of a biphasic region should provide an ultimate test for the applicability of Onsager's theory. This lack of detection of the coexistence may result from a too narrow range of clay concentration. As shown in Figure 11, the temperature variation of the ^{23}Na longitudinal relaxation rates totally agrees with the condition of fast exchange between the different environments accessible to the sodium counterions. As a consequence, a single spin population is detected by ^{23}Na NMR at the time scale of NMR (typically 10^{-3} s).[19,21] In order to remain under this condition of fast exchange, if two phases coexist within the dispersion, with a significant difference of their clay concentrations and thus their corresponding ^{23}Na relaxation rates,[19,21] the spatial extent of the corresponding domains should not exceed 1 μm, explaining the lack of direct visual detection.

Another question concerns the origin of the clay ordering. Since the clay directors within the dense samples are macroscopically oriented parallel to the compression axis, we do not expect that the clay orientation is induced by the flow of the solvent occurring during the compression. A further confirmation of that conclusion is given by the isotropic sample at the Laponite concentration 6.2% w/w which is also prepared by uniaxial compression. If the clay orientation is induced during the compression by some hydrodynamical effects, this sample should also be macroscopically oriented. The appearance of the initial clay organization is also interesting: do ordered microdomains form spontaneously within the whole volume[53] of the sample or do they nucleate from some borders[54] (the piston head or the bottom of the cylinder)? Direct optical detection by birefringence measurement during the compression should help to elucidate that question.

IV. Conclusions

Aqueous dispersions of anisotropic charged colloids (Laponite synthetic clay) were used as a model to probe the isotrope/nematic first-order phase transition predicted by Onsager for solids bodies. By using ^{23}Na nuclear magnetic resonance

spectroscopy and ^{1}H pulsed field gradient echo attenuation, we detected the occurrence of a macroscopic ordering at a critical clay concentration (7% w/w) significantly higher than the value reported from birefringence measurements on the same dispersions in capillary tubes. Furthermore, our nuclear magnetic resonance measurements exhibit a very progressive ordering of the clay dispersion which may results from many factors (particle size and shape heterogeneity, competition between electrostatic and excluded volume effects) without invalidating the isotrope/nematic phase transition predicted by Onsager.

Acknowledgment. We cordially thank Drs. P. Levitz, L. Michot, J. Puibasset, and R. Setton for helpful discussions. NMR spectrometers used in this study were purchased thanks to Grants from Région Centre (France).

References and Notes

(1) van der Schoot, P.; Michels, M. A.; Brunsveld, L.; Sijbesma, R. P.; Ramzi, A. *Langmuir* **2000**, *16*, 10076.
(2) Dvinskikh, S. V.; Furo, I. *Langmuir* **2001**, *17*, 6455.
(3) Galindo, A.; Haslam, A. J.; Varga, S.; Jackson, G.; Vanakaras, A. G.; Photinos, D. J.; Dunmur, D. A. *J. Chem. Phys.* **2003**, *119*, 5216.
(4) Adams, M.; Dogic, Z.; Keller, S. L.; Fraden, S. *Nature* **1998**, *393*, 349.
(5) Clore, G. M.; Starich, M. R.; Gronenborn, A. M. *J. Am. Chem. Soc.* **1998**, *120*, 10571.
(6) Purdy, K. R.; Dogic, Z.; Fraden, S.; Rühm, A.; Lurio, L.; Mochrie, S. G. J. *Phys. Rev. E* **2003**, *67*, 31708.
(7) Wierenga, A.; Philipse, A. P.; Lekkerkerker, H. N. W. *Langmuir* **1998**, *14*, 55.
(8) Pelletier, O.; Davidson, P.; Bourgaux, C.; Coulon, C.; Regnault, S.; Livage, J. *Langmuir* **2000**, *16*, 5295.
(9) Michot, L. J.; Ghanbaja, J.; Tirtaatmadja, V.; Scales, P. J. *Langmuir* **2001**, *17*, 2100.
(10) Bihannic, I.; Michot, L. J.; Lartiges, B. S.; Vantelon, D.; Labille, J.; Thomas, F.; Susini, J.; Salomé, M.; Fayard, B. *Langmuir* **2001**, *17*, 4144.
(11) Onsager, L. *Ann. N. Y. Acad. Sci.* **1949**, *51*, 627.
(12) Gabriel, J.-C. P.; Sanchez, C.; Davidson, P. *J. Chem. Phys.* **1996**, *100*, 11139.
(13) Mourchid, A.; Lécolier, E.; Van Damme, H.; Levitz, P. *Langmuir* **1998**, *14*, 4718.
(14) DiMasi, E.; Fossum, J. O.; Gog, T.; Venkataraman, C. *Phys. Rev. E.* **2001**, *64*, 61704.
(15) Lemaire, B. J.; Panine, P.; Gabriel, J. C. P.; Davidson, P. *Europhys. Lett.* **2002**, *59*, 55.
(16) Bhatia, S.; Barker, J.; Mourchid, A. *Langmuir* **2003**, *19*, 532.
(17) Mourchid, A.; Delville, A.; Lambard, J.; Lécolier, E.; Levitz, P. *Langmuir* **1995**, *11*, 1942.
(18) Levitz, P.; Delville, A.; Lécolier, E.; Mourchid, A. *Prog. Colloid Polym. Sci.* **2001**, *118*, 290.
(19) Porion, P.; Faugère, M. P.; Lécolier, E.; Gherardi, B.; Delville, A. *J. Phys. Chem. B* **1998**, *102*, 3477.
(20) Porion, P.; Rodts, S.; Al-Mukhtar, M.; Faugère, A. M.; Delville, A. *Phys. Rev. Lett.* **2001**, *97*, 208302.
(21) Porion, P.; Al-Mukhtar, M.; Faugère, A. M.; Pellenq, R. J. M.; Meyer, S.; Delville, A. *J. Phys. Chem. B* **2003**, *107*, 4023.
(22) Delville, A.; Levitz, P. *J. Phys. Chem. B* **2001**, *105*, 663.
(23) Meyer, S.; Levitz, P.; Delville, A. *J. Phys. Chem. B* **2001**, *105*, 10684.
(24) Balnois, E.; Durand-Vidal, S.; Levitz, P. *Langmuir* **2003**, *19*, 6633.
(25) Porion, P.; Al-Mukhtar, M.; Meyer, S.; Faugère, A. M.; van der Maarel, J. R. C.; Delville, A. *J. Phys. Chem. B* **2001**, *105*, 10505.
(26) Thompson, D. W.; Butterworth, J. T. *J. Colloid Interface Sci.* **1992**, *151*, 236.
(27) Van der Maarel, J. R. C.; Jesse, W.; Hancu, I.; Woessner, D. E. *J. Magn. Reson.* **2001**, *151*, 298.
(28) Van der Maarel, J. R. C. *Concepts Magn. Reson., Part A* **2003**, *19A*, 97.
(29) Bull, T. E. *J. Magn. Reson.* **1972**, *8*, 344.
(30) Callaghan, P. T. *Principles of Nuclear Magnetic Resonance Microscopy*; Clarendon Press: Oxford, 1991.
(31) Nakashima, Y. *Clays Clays Miner.* **2003**, *51*, 9.
(32) Delville, A.; Porion, P.; Faugère, A. M. *J. Phys. Chem. B* **2000**, *104*, 1546.
(33) Ernst, R. R.; Bodenhausen, G.; Wokaum, A. *Principles of Nuclear Magnetic Resonance in One and Two Dimensions*; Clarendon Press: Oxford, 1987.
(34) Müller, N.; Bodenhausen, G.; Ernst, R. R. *J. Magn. Res.* **1987**, *75*, 297.
(35) Knubovets, T.; Shinar, H.; Navon, G. *J. Magn. Res.* **1998**, *131*, 92.
(36) Grandjean, J.; Robert, J. L. *J. Magn. Res.* **1999**, *138*, 43.
(37) Oosawa, F. *J. Polym. Sci.* **1957**, *23*, 421.
(38) Manning, G. S. *Acc. Chem. Res.* **1979**, *12*, 443.
(39) Delville, A. *J. Phys. Chem. B* **1999**, *103*, 8296.
(40) Delville, A. *J. Phys. Chem. B* **2002**, *106*, 7860.
(41) Eppenga, R.; Frenkel, D. *Mol. Simul.* **1984**, *52*, 1303.
(42) Forsyth, P. A.; Marcelja, S., Jr.; Mitchell, D. J.; Ninham, B. W. *Adv. Colloid Interface Sci.* **1978**, *9*, 37.
(43) Stroobants, A.; Lekkerkerker, H. N. W.; Odijk, Th. *Macromolecules* **1986**, *19*, 2232.
(44) Kramer, E. M.; Herzfeld, J. *Phys. Rev. E* **2000**, *61*, 6872.
(45) Wensik, H. H.; Vroege, G. J.; Lekkerkerker, H. N. W. *J. Chem. Phys.* **2001**, *115*, 7319.
(46) Viamontes, J.; Tang, J. X. *Phys. Rev. E* **2003**, *67*, 40701(R).
(47) Delville, A. *Langmuir* **2003**, *19*, 7094.
(48) Meyer, S.; Levitz, P.; Delville, A. *J. Phys. Chem. B* **2001**, *105*, 9595.
(49) Speranza, A.; Sollich, P. *Phys. Rev. E* **2003**, *67*, 61702.
(50) Bates, M. A. *J. Chem. Phys.* **1999**, *111*, 1732.
(51) Caprion, D.; Bellier-Castella, L.; Ryckaert, J. P. *Phys. Rev. E* **2003**, *67*, 41703.
(52) Dubois, M.; Zemb, Th.; Belloni, L.; Delville, A.; Levitz, P.; Setton, R. *J. Chem. Phys.* **1992**, *96*, 2278.
(53) Van der Beek, D.; Lekkerkerker, H. N. W. *Europhys. Lett.* **2003**, *61*, 702.
(54) Shioda, T.; Wen, B.; Rosenblatt, Ch. *Phys. Rev. E* **2003**, *67*, 41706.